

**In vitro biocompatibility of mesoporous metal (III; Fe, Al, Cr) trimesate MOFs nanocarriers**

Journal:	<i>Journal of Materials Chemistry B</i>
Manuscript ID	TB-ART-06-2015-001223.R1
Article Type:	Paper
Date Submitted by the Author:	09-Sep-2015
Complete List of Authors:	Grall, Romain; CEA, IRCM/SREIT/LCE Hidalgo-Crespo, Tania; Institut Lavoisier (CNRS 8180), Université de Versailles Saint Quentin Delic, Jozo; CEA, IRCM/SREIT/LCE Garcia-Marquez, Alfonso; Institut Lavoisier (CNRS 8180), Université de Versailles Saint Quentin horcajada, patricia; Institut Lavoisier (CNRS 8180), Université de Versailles Saint Quentin Chevillard, Sylvie; CEA, IRCM/SREIT/LCE

***In vitro* biocompatibility of mesoporous metal (III; Fe, Al, Cr) trimesate MOFs nanocarriers**

Romain Grall^a, Tania Hidalgo,^b Jozo Delic,^a Alfonso Garcia-Marquez,^b Sylvie Chevillard^{a*} and Patricia Horcajada^{b*}

^aLaboratoire de Cancérologie Expérimentale, Service de Radiobiologie Expérimentale et Innovations Technologiques, Commissariat à l'Energie Atomique (CEA), Fontenay-aux-Roses, 8 Route du Panorama, 92265 Fontenay-aux-Roses, France.

^bInstitut Lavoisier, CNRS UMR 8180, Université de Versailles Saint-Quentin-en-Yvelines, 45 Av. des Etats-Unis, 78035 Versailles cedex, France.

* Co-last authors and corresponding authors

ABSTRACT

The high porosity and versatile composition of the benchmarked mesoporous metal(Fe, Al, Cr) trimesate metal-organic frameworks (MIL-100(Fe, Al, Cr)) make them very promising solids in different strategic industrial and societal domains (separation, catalysis, biomedicine, etc). In particular, the MIL-100(Fe) nanoparticles (NPs) have recently revealed as a one of the most promising and innovative next generation tools enabling multidrug delivery to overcome cancer resistance. Here, we analyzed the *in vitro* toxicity of the potential drug nanocarrier MIL-100(Fe) NPs and the effect of the constitutive cation by comparing its cytotoxicity with that one of its Cr and Al analogue NPs. Lung (A549 and Calu-3) and hepatic (HepG2 and Hep3B) cell lines were selected considering pulmonary, ingestion or intravenous exposure modes. First, the complete physicochemical characterization (structural, chemical and colloidal stability) of the MIL-100(Fe, Al, Cr) NPs was performed in the cell culture media. Then, their cytotoxicity was evaluated on the four selected cell lines using a combination of methods from cell impedance, cell survival/death and ROS generation to DNA damage for measuring genotoxicity. Thus, MIL-100(Fe, Al, Cr) NPs did not induce *in vitro* cell toxicity, even at high doses in the p53 wild type cell lines (A549) and calu-3 (lung) and HepG2 (liver)). The only toxic effect of MIL100-Fe was observed in the hepatocarcinoma cell line Hep3B, which is stress sensitive because it does not express TP53, the guardian of the genome.

1. Introduction

Exceptional and regular porosities together with an extraordinary structural and compositional versatility have made Metal-Organic Frameworks (MOFs) very promising candidates for industrially and societally relevant domains (separation, catalysis, sensing, etc.)¹⁻¹¹. The recent emergence of nanometric porous MOFs (nanoMOFs) in the biomedical field have attracted a great interest owing to their amphiphilic internal microenvironment, well-adapted to the adsorption of diverse guests (drugs, biological gazes, cosmetics, nucleic acids)^{5, 12-16}. Of particular relevance is the development of highly efficient and biocompatible nanocarriers for cancer treatment^{17, 18}. However, important toxicological concerns have arose from these promising applications, notably in biomedicine. The physicochemical properties of nanoMOFs (composition, size, molecular weight, surface chemistry...) might play a key role

in the nanomaterial's performance in terms of biocompatibility, biodistribution, and biodegradability and hence, toxicity and efficacy¹⁹⁻²⁴.

Therefore, prior to any bioapplication of nanoMOFs, it is of high relevance to investigate their toxicity profile²⁵. To the best of our knowledge, only two studies have been reported dealing with the *in vivo* toxicity of few nanoMOFs. Few of us reported for the first time the evaluation of the *in vivo* toxicity of high doses (220 mg.kg⁻¹) of three Fe-nanoMOFs based on different polycarboxylate ligands [(MIL-100 (trimesate), MIL-88A (fumarate) and MIL-88B_4CH₃ (tetramethylterephthalate)]²⁶ administered intravenously to rats, evidencing a lack of severe toxicity (behavioral, histological, biochemical, enzymatic parameters, etc.) from 1 day to up to 3 months. Besides, the nanoMOF biodegradation into their constitutive components (linker and iron) was confirmed, observing an excretion via urine and feces without any metabolization. These very encouraging results have opened new perspectives for improving treatments in nanomedicine based on nanoMOFs^{26, 27}. Despite these promising results obtained with few iron carboxylates and due to the high versatility of these solids, many factors could influence their toxicity such as their topology, composition, biological stability, particle size and surface properties, among others. Therefore, the understanding of the main parameters governing the toxicity of nanoMOFs is of high relevance. In this sense, a second work dealing with the screening of the *in vivo* toxicity of nine nanoMOFs with different structures and compositions in zebrafish embryos was recently reported by Ruyra *et al.*²⁸, concluding a wide variation of the toxicity of the different nanoMOFs and highlighting the influence of the cation leaching coming from the hybrid network degradation.

Given the great variety and number of nanoMOFs and their application domains²⁹⁻³⁴, it is impossible to study their toxicity using *in vivo* assays for ethical, temporal and economic reasons. *In vitro* studies are an interesting alternative to screen the nanoMOF toxicity, providing additional mechanistic insights into toxicity pathways. In fact, cytotoxicity of a series of porous nanoMOFs with different compositions and structures have been recently evaluated in different cell lines (J774, HeLa, Caco-2, HL-60, HepG2, MCF7...),^{28, 35-37} concluding that (i) the MOFs NPs exhibit lower cytotoxicity as compared to that of other commercialized nanosystems, and (ii) a strong dependence between the MOF composition and the cytotoxicity occurs. In particular, Co-, Ni- or Mg-based nanoMOFs showed no marked cytotoxicity on HepG2 and MCF7 cells, whereas nanoMOFs containing Cu, Mn or Zn seemed to be highly cytotoxic (at 200 μ M). In addition, the cellular specific response obtained after exposure with different nanoMOFs, clearly indicated cell line specific

responses due to both cellular origin and genetic background. Among the nanoMOFs, the mesoporous metal(III) trimesate MIL-100 series (MIL stands for Material of Institut Lavoisier) is particularly interesting. Their cubic structure based on trivalent metal octahedra (Fe³⁸, Al³⁹, Cr⁴⁰, V⁴¹, Sc⁴², Tb⁴³) trimers linked to trimesate anions exhibits an important porosity (BET surface area and pore volume of 2400 m².g⁻¹ and 1.2 cm³.g⁻¹, respectively) associated to two types of mesoporous cages (~25 and 29 Å) accessible by microporous windows (~5 and 8.5 Å). Their high thermal (300 °C) and chemical stability (organic solvent, water under reflux) together with the presence of unsaturated Lewis acid metal sites (CUS) or, even, redox sites^{44, 45}, make them interesting candidates for a vast number of domains such as CO₂ capture⁴⁶, H₂ storage⁴⁷, gas separation⁴⁵, catalysis³⁸, xylene separation⁴⁸, N/S compound removal⁴⁹, energy-efficient dehumidification⁵⁰, drug delivery and imaging^{51, 52} and so on. Notably, the MIL-100(Fe) has revealed as one of the most promising drug nanocarrier due to (i) its exceptional loading capacity of several therapeutic molecules, (ii) their controlled release and (iii) its advantageous imaging properties.

In the present work, considering the promising outcomes of the MIL-100 NPs, a selection of three MIL-100 nanoparticulate systems based on different metals (Fe, Al, Cr) has been tested for *in vitro* toxicity in order to (i) understand the more relevant mechanisms involved on the MIL-100 NPs toxicity, in particular, the role of the cation release. In this sense, the nature of the cation could either damage the cells, through the formation of reactive oxygen species (ROS), or at the opposite, could favor the interaction and neutralization of ROS. Overall, the presence of the cation could alter the cellular homeostasis⁵³⁻⁵⁷; and ii) reveal attractive features for future applications in relevant fields, notably biomedicine thought their administration by inhalation, intravenous and gastro-intestinal routes. In addition, pulmonary route is one of the major exposure modes to NPs. Thus, cytotoxicity studies were conducted on a series of four human epithelial cell lines chosen to mimic targeted tissues (*i.e.* lung and liver). Thus, two lung (A549 and Calu-3) and two hepatic cell lines (HepG2 and Hep3B) were tested, selecting the Hep3B as the only one that does not express p53 (the guardian of the genome), which allows estimating NPs toxicity in a highly stress sensitive context.

2. Experimental section

2.1 Materials.

Iron(III) chloride hexahydrate (97 %), 1,3,5-benzene tricarboxylic acid (trimesic acid; 95 %), aluminium(III) nitrate nonahydrate (99.9%), trimethyl-1,3,5-trimesate, phosphate buffered saline (PBS) solution (0.01 M, pH=7.4), chromium(III) nitrate nonahydrate were purchased from Sigma-Aldrich. Ethanol (96 %) and methanol (99.9%) were obtained from VWR.

Nitric acid, ((R)-(-)-4-(3-aminopyrrolidino)-7-nitrobenzofurazan (furazan). Similarly, 2',7'-dichlorofluorescein diacetate (2.5 μ M; DCFH-DA), L-glutamine (2 mM), Tris/EDTA (10 mM, pH 7.4) were purchased from Life Technologies. Heat-inactivated fetal bovine serum (FBS), dimethylsulfoxide (DMSO; \geq 99.7 %) and penicillin/streptomycin (100 U.mL⁻¹) were provided by Fischer. Lipopolysaccharide (LPS; InvivoGen, San Diego, CA), phorbol 12-myristate-13-acetate (PMA; Abcam, Biochemicals). All materials were used as received without further purification.

2.1.1 Synthesis and characterization of MIL-100(Fe, Al, Cr) NPs

2.1.1.1 Synthesis of MIL-100(Fe) NPs. MIL-100(Fe) NPs were synthesized following a microwave-assisted hydrothermal method according to a previously reported procedure⁵⁸. 2.43 g (9.01 mmol) of iron(III) chloride hexahydrated and 0.84 g (4.00 mmol) of trimesic acid were dissolved in 30 mL of distilled water. The reaction was treated with a heating ramp of 30 seconds to 130 °C and then, maintained for 5 minutes and 30 seconds (1600 W). Activation or purification of MIL-100(Fe) NPs consisted of successive washing steps by centrifugation (14500 rpm, 10 min) and re-dispersion of the NPs in aliquots of water (once) and absolute ethanol (5 times). Further activation was carried out by re-dispersing 2.5 g of the NPs in 20 mL of an aqueous KF solution (0.1 M). Then, the suspension was stirred for 1 h 40 min under stirring and ambient conditions. Finally, NPs were collected by centrifugation (14500 rpm, 10 min) and washed two times with 20 mL of water and once with 20 mL of absolute ethanol. Activated MIL-100(Fe) NPs were stored wet with few droplets of absolute ethanol⁵⁹.

2.1.1.2 Synthesis of MIL-100(Al) NPs. MIL-100(Al) NPs were hydrothermally synthesized by a microwave-assisted route as mentioned before⁵⁸. Briefly, a solution of 1.43 g (5.68 mmol) of aluminum nitrate nonahydrate, 1.21 g (4.82 mmol) of trimethyl-1,3,5- trimesate and 4 mL of nitric acid (4 M) were dissolved in 20 mL of distilled water under vigorous stirring. The reaction was heated at 210°C for 30 min using a hydrothermal microwave-assisted

method (400 W). The resulting mixture was cooled down with an ice bath and recovered by centrifugation (10500 rpm, 20 min). MIL 100(Al) NPs were then activated by dispersing the collected NPs into 50 mL of methanol overnight under vigorous stirring. The activated solid was recovered by centrifugation at 10500 rpm for 20 min, exchanged twice with ethanol and kept wet for storage.

2.1.1.3 Synthesis of MIL-100(Cr) NPs. The synthesis of MIL-100(Cr) NPs was carried following a previously reported microwave-assisted hydrothermal method⁵⁸. 2.40 g (5.99 mmol) of chromium nitrate nonahydrated and 0.84 g (4.00 mmol) of trimesic acid were dissolved in 30 mL of distilled water under moderate stirring. The reaction was thermally treated with a heating ramp of 4 minutes to 200 °C (800 W) and kept at this temperature for one minute. The resulting mixture was cooled down with an ice bath and dispersed in 20 mL of water, being centrifuged after (10500 rpm, 15 min). The activation of MIL-100(Cr) consisted on the dispersion of 500 mg of the recovered as-synthesized solid in 20 mL of ethanol for 5 min and centrifuged at 4000 rpm for 15 min. From the liquid fraction obtained, a new centrifugation is performed (10500 rpm, 20 min), keeping the solid and re-dispersing it in 20 mL of ethanol and centrifuged once again. This procedure was repeated two more times.

Prior to use, the MIL-100(Fe, Al, Cr) NPs were redispersed in 50 mL of the selected solvent, the solid was recovered by centrifugation at 10500 rpm for 15 minutes and the liquid fraction discarded. Note that for the experiments NPs were weighted wet based on the wet: dry ratio previously determined from NPs dry at 100 °C overnight.

2.1.2 Encapsulation of furazan. The encapsulation of ((R)-(-)-4-(3-aminopyrrolidino)-7-nitrobenzofurazan (here called furazan) was performed according to a previously reported procedure³⁷. Briefly, furazan was encapsulated by soaking 50 mg of the NPs (based on the dried weight) in 10 mL of a furazan containing solution (0.3 mg·mL⁻¹) under vigorous stirring for 2 h at room temperature. The furazan@NPs were recovered by centrifugation (15000 rpm, 10 min) and five times washed with 10 mL of water.

2.1.3 Physicochemical characterization. Dynamic Light Scattering (DLS) distribution and ζ -potential were analyzed by on a Zetasizer Nano (Malvern Instruments). Size is given as the mean size distribution corresponding with the hydrodynamic diameter of the NPs. Samples

were prepared by dispersing the NPs at $0.1 \text{ mg}\cdot\text{mL}^{-1}$ in the desired media by using an ultrasound tip (30 % amplitude for 30 s; Digital Sonifer 450, Branson). Fourier transform infrared (FTIR) spectra were collected using a Nicolet 6700 instrument (Thermo scientific, USA) in the $4000\text{-}400 \text{ cm}^{-1}$ range using powdered samples. Thermogravimetric analyses (TGA) were performed on a Perkin Elmer Diamond TGA/DTA STA 6000 in the $25\text{-}600 \text{ }^\circ\text{C}$ temperature range under a $3 \text{ }^\circ\text{C}\cdot\text{min}^{-1}$ scan rate and O_2 flow of $20 \text{ mL}\cdot\text{min}^{-1}$. X-Ray powder diffraction (XRPD) patterns were collected using a high-throughput D8 Advance Bruker diffractometer working on transmission mode and equipped with a focusing Göbel mirror producing Cu $\text{K}\alpha_1$ radiation ($\lambda = 1.54056 \text{ \AA}$) and a Lynxeye detector. Data were collected at room temperature in the $2^\circ < 2\theta < 30^\circ$ range with a step width of 0.02° . N_2 sorption isotherms were obtained at 77 K using a BELsorp Maxi (Bel, Japan). Prior to the analysis, *ca.* 30 mg of dry sample were outgassed under primary vacuum at $140 \text{ }^\circ\text{C}$ for 3h.

2.1.4 Quantification of trimesic acid by high performance liquid chromatography (HPLC). Release of the trimesic acid was monitored in a reversed phased HPLC system Waters Alliance E2695 separations module from Waters with a Sunfire-C18 reverse-phase column ($5\mu\text{m}$, $4.6\times 150 \text{ mm}$ from Waters) and equipped with a variable-wavelength photodiode array detector Waters 2998 and controlled by Empower software. The mobile phase consisted of a mixture of 45 % v/v methanol in PBS solution (0.04 M , pH 2.5), injecting $50 \mu\text{L}$ as sample volume under a flow rate at $1 \text{ mL}\cdot\text{min}^{-1}$ and $25 \text{ }^\circ\text{C}$ column-temperature. The standards used for the calibration curve consisted of trimesic acid solutions in the different complete cell culture media (FBS supplemented-DMEM and -MEM) with a concentration range from 25.00 to $0.39 \mu\text{g}\cdot\text{mL}^{-1}$ (correlation coefficient > 0.99). Chromatogram of standards showed a retention time for the trimesic acid of 3.6 min with an absorption maximum at 215 nm. Degradation kinetics of the NPs were obtained in the different media (FBS supplemented-DMEM and -MEM) at $37 \text{ }^\circ\text{C}$ according to a previously reported procedure⁶⁰ and represented as the wt % of the linker released, considering the maximum of degradation of 100 % when the total amount of the linker was released in the medium.

2.1.5 Colloidal stability tests. MIL-100(Fe, Al, Cr) NPs were dispersed at $0.5 \text{ mg}\cdot\text{mL}^{-1}$ in FBS supplemented-DMEM or -MEM by using an ultrasound tip (30 % amplitude for 30 s). Evolution of the NP mean size distribution and the surface charge were followed as a function of time by dynamic light scattering (DLS) and ζ -potential.

2.2 *In vitro* studies.

2.2.1 Cell lines and cell culture.

The human A549 cell line (ATCC[®]CCL-185[™]) was routinely grown in Dulbecco's modified Eagle medium (DMEM) with glutamax supplemented with 10% (v/v) inactivated fetal bovine serum (FBS) and 1 mM antibiotic-antimycotic (Invitrogen, Carlsbad, CA). This medium is considered complete DMEM. Human Hep3B cells (ATCC number[®]HB-8064[™]), HepG2 cell line (ATCC number[®]HB-8065[™]) and Human Calu-3 cell line (ATCC number[®]HTB-55[™]) were cultured at 37°C in a humidified atmosphere of 5% CO₂ and 95% air, cultured in modified Eagle medium (MEM) supplemented with 10% (v/v) inactivated fetal bovine serum.

Human Calu-3 cells (ATCC number[®]HTB-55[™]) were also maintained at 37°C in a humidified atmosphere of 5% CO₂ and 95% air using modified Eagle medium (MEM) supplemented with 15% (v/v) inactivated fetal bovine serum, 5 mL of 200 mM L-glutamine (Sigma-Aldrich, St Louis, MO), 1% (v/v) 100 mM sodium pyruvate (Sigma-Aldrich), 1% (v/v) 1 M HEPES (Sigma-Aldrich) and 1 mM antibiotic-antimycotic (Invitrogen). This medium is also considered to be complete MEM

2.2.2 Cell exposure.

MILs NPs were suspended in water and dispersed. This suspension was diluted in appropriate culture medium to obtain final concentrations for cell treatment. Cells were exposed for 2 and 24 h with MIL-100 NPs final concentrations from 6 to 64 µg/cm² (corresponding to 10 to 100 µg/mL), depending on the assay. Test concentrations were selected according to previous studies^{5, 51} performed *in vivo* and were dramatically increased in order to attest the toxicity or the absence of toxicity at ultra-high doses.

2.2.3 xCELLigence[®] (real-time follow-up).

Impedance measurements principle has been well described in our previous studies⁶¹. Adherents A549 and Hep3B cell lines were seeded 24h in E-plates prior the assay at a density of 5x10³ cells *per* well, whereas Calu-3 and HepG2 cell line were plated 48h before the treatment at a density of 15x10³ cells and 10x10³ cells/well respectively. After 30 min of incubation at 37°C, the cells were placed in a Real-Time Cell Analyzer (RTCA) station (ACEA Biosciences, San Diego, CA). During the first 24h, the impedance was measured every 5 min for 6 h (corresponding with *adhesion phase*) and after this time, the measurement was performed every 10 min (proliferation phase). After at least 24h of growth, different concentration of MIL-100s NPs (6, 32 and 64 µg/cm²) were exposed to cells and monitored

the impedance every 5 min for 6 h (corresponding as *early effects*), and then every 10 min for 74 h (known as *late effects*). The background of the E-plates (specific 96 wells microplates covered with electrodes; ACEA Biosciences, San Diego, CA) was determined as control where 150 μL of each cell suspension was added in a final volume of 200 μL of media.

2.2.5 Measurement of MIL-100-cell interactions, cell death, and NP release

Following 2 and 24 h treatments of the tested cell lines with MIL-100 NPs, supernatants were collected and the cells were trypsinized for 5 min. Trypsin was inactivated by the addition of complete medium, collected, and added to the corresponding supernatant. The tubes were then centrifuged for 5 min at 300 \times g and the pellet was resuspended in 500 μL of PBS (+MgCl₂, +CaCl₂) containing 5% FBS and then transferred to flow cytometry-compatible tubes (BD Biosciences; Franklin Lakes, NJ). Multi-parametric analyses were performed on a BD FacsCalibur using FlowJo 7.5.5 software (Ashland, OR). An initial analysis was done on size/granulometry parameters to collect living and dead cells and to remove fragmented cells. Granulometry parameter is given by the SSC channel (Side Scatter Channel) and the interaction between NPs and cells is proportional to an increase of the SSC, as previously described by Zucker and colleagues⁶². This first step allowed us to determine the gate where at least 2×10^4 events per replica were recorded. Upon these gated events, the To-Pro3 (Molecular Probes[®], Invitrogen; Carlsbad, CA) signal was subsequently collected on FL4 (λ_{em} : 661/16 nm) after He-Ne laser excitation at 635 nm and was used for the analysis of cell viability since this dye is compatible with the equipment and with nanoparticle detection. The results were reported as the mean distribution of the cells combining SSC and To-Pro3 measurements as described in our previous study⁶¹.

2.2.6 MIL-100 NPs internalization using confocal videomicroscopy. For each experiment, 40×10^4 Calu-3 cells were plated on 14 mm uncoated glass bottom dishes (Ref P12G-1.5-14-F, MatTek) for at least 48 h prior to the experiment. The cells were then treated at different times (15 min, 24 h) with MIL-100 NPs at concentrations of 6 and 64 $\mu\text{g}/\text{cm}^2$. Fluorescent images were captured through a Plan Fluor 63X objective (NA: 1.4) on a Nikon A1 confocal laser scanning videomicroscope. Images have been acquired sequentially every 10 min up to 24h with a pixel format of 1200 x 1200 and a resolution in the x,y dimensions of 60 nm/pixel and 0.3 μm /pixel in the z dimension.

2.2.7 Measurement of ROS level

The cells were seeded in 6-well plate (TPP) 24h before the treatment exposure at different cell density (15×10^4 cells with A549 cells, 40×10^4 cells in Calu-3 cell line, 30×10^4 in case of HepG2 cells and 10×10^4 Hep3B cells). The medium was replaced with the different concentrations of MIL-100. Cells treated with H_2O_2 (mixed with PBS ($^+MgCl_2$, $^+CaCl_2$) containing 5% FBS) during 15 min were considered as positive control for all four cell lines, whereas non-treated cells were considered as negative control negative. After 15min of incubation time, supplier's instructions were followed to measure ROS intra-cellular level with CM- H_2 DCFDA probe (Life Technologies). Acquisitions were performed on a BD FacsCalibur using CellQuest Pro software and then monoparametric analyses were performed using FlowJo 7.5.5 software. During the acquisitions, the initial analysis was done using size/granulometry parameters. This first step allowed us to determine the gate where at least 2×10^4 events *per* replica were recorded. Finally upon these gated events, the CM- H_2 DCFDA (Molecular Probes®, Invitrogen; Carlsbad, CA) signal was collected using the FL1 channel (λ_{em} : 525/50 nm) after an air-cooled Argon Ion laser excitation at 488 nm (15 mW).

2.2.8 Cell cycle analysis.

Adherents cell lines were put in contact with at different incubations times (2 and 24 h) with MILs NPs. After each time, the cells were washed and trypsinized for 5 min. Trypsin was inactivated by adding complete medium, cells were centrifuged for 5 min at $300 \times g$. After the centrifugation, the cells were resuspended in 1 mL of PBS ($^+MgCl_2$, $^+CaCl_2$, containing 5% FBS). The resuspended cells were then fixed via the dropwise addition of 3 mL of 70% ethanol and the tubes were placed at $-20^\circ C$ overnight. The fixed cells were then centrifuged for 5 min at $300 \times g$ and resuspended with 300 μL of mix containing [PBS ($^+MgCl_2$ $^+CaCl_2$) + 5% of FBS + ToPro3 (at 0.5 μM final) + RNase A (50 $\mu g/mL$ final)] in each tube. Finally, the tubes were kept at $4^\circ C$ for 30min to adequately stain of the DNA. Mono-parametric analyses were performed the next day on a BD FacsCalibur using FlowJo 7.5.5 software. The first analysis was done using size/granulometry parameters, allowing us to determine the gate where 2×10^4 events *per* replica were recorded. Upon these gated events, the ToPro3 signal (Molecular Probes®, Invitrogen Carlsbad, CA) was collected on the FL4 channel (λ_{em} : 642/61 nm) He-Ne laser excitation at 635 nm. The FL4 signal was plotted as FL4-W vs FL4-A in a dot-plot graph which allowed to discriminate doublets (e.g. a G1 doublet from a G2/M single) or cellular aggregates⁶³. The results were reported as the mean distribution.

2.2.9 Genotoxicity through the measurement of γ -H2Ax-foci. Hep3B cell line was seeded in 8-well plate (Lab-Tek™ II Chamber Slide™ (Nunc) 24 h before exposure with the stimulus. The NPs treatments were prepared at doses of 6 and 64 $\mu\text{g}/\text{cm}^2$ and put it in contact with cells for 24 h. After this incubation time, the protocol applied is already described in detail in our previous study⁶¹. The quantification of γ -H2Ax foci was performed by confocal microscopy, as described in previous studies⁶¹.

2.2.10 Statistical analysis. The statistical analysis selected for xCELLigence® analysis, MILs NP/cell interactions measurements by flow cytometry and cell cycle analysis, a Student's t-test was performed for each exposure condition compared to non-exposed cells. In case of the quantification and number comparison of γ -H2Ax foci, Wilcoxon rank test was employed based on 200 observations for each condition.

3. Results and discussion

3.1 Synthesis and physicochemical characterization of MIL-100(Fe), MIL-100(Al) and MIL-100(Cr) NPs

First, the synthesis of MIL-100 NPs based on different trivalent cations (Fe, Al or Cr) was successfully performed using an efficient and green microwave-assisted hydrothermal route^{58, 59}. These NPs were fully characterized by different techniques, including X-ray powder diffraction (XRPD), dynamic light scattering (DLS), ζ -potential and transmission electron microscopy (TEM), in order to provide qualitative and quantitative parameters to associate to their potential cytotoxicity. XRPD patterns (Figure 1) show the characteristic diffraction peaks of the MIL-100 structure, with however broad reflections in agreement with the presence of small crystals. TEM images (Figure 1) show well-faceted NPs for MIL-100(Fe) and (Al) of around 150 and 300 nm diameter. In contrast, more or less spherical and smaller NPs (~25 nm) are observed for the MIL-100(Cr), with however an important aggregation between them.

The analysis of the particle size and ζ -potential was initially performed in water and ethanol suspensions, showing in all cases quite monodispersed particles (Table 1). Particle size of MIL-100(Fe) and (Al) NPs is in agreement with the TEM observations (~150 and 300 nm, respectively). The larger particle size of MIL-100(Cr) NPs in comparison with the microscopy

images (80 ± 41 vs. ~ 25 nm, respectively) seems to be related with an important aggregation phenomenon in the colloidal solution, as already observed in the dry state (Figure 1).

Except for the MIL-100(Fe) NPs, in which the particle size was not significantly different in both solvents (139 ± 25 and 168 ± 10 nm in water and ethanol, respectively), the dimension of MIL-100(Al, Cr) NPs seems to be larger when dispersed in water than in ethanol (249 ± 28 vs. 237 ± 41 nm and 142 ± 63 vs. 80 ± 41 nm for the MIL-100(Al) and (Cr), respectively). This might be related with the lower absolute value of the surface charge (Table 1). It is well-known that absolute ζ -potential values closer to the neutral charge (usually $< [30]$ mV) lead to higher aggregation effect as a consequence of the absence of enough electrostatic repulsions to stabilize the colloids. Additionally, it was previously proposed that this aggregation phenomenon could be associated with a higher dynamic formation of the MOF in water than in ethanol solutions⁵⁸.

Regarding the ζ -potential measurements, the external surface of these MIL-100(Fe, Al, Cr) NPs would be rationally formed from a combination of partially coordinated carboxylate/carboxylic acids and metal octahedra trimers, whose coordination sphere could typically be ensured by trimesate moieties and OH^- , F^- or H_2O terminal groups. The negative charge associated to the MIL-100(Fe) surface in both solvents suggests a higher proportion of iron than carboxylate/carboxylic acid, in agreement with previously reported NPs treated with KF (see experimental section)⁵⁹. This KF treatment, used for the complete removal of non-reacted ligand, provoke the replacement of partially coordinated linkers on the outer surface by F^- anions to the metallic centers, leading to negative charges. In contrast, the highly positive superficial charges obtained in ethanol solutions of MIL-100(Al) and (Cr) NPs as well as their slightly positive or negative ζ -potential values in water, respectively, might indicate the presence on their outer surfaces of an important fraction of linkers, either pending carboxylate and/or carboxylic acid groups (Table 1). The acidification of the pH when NPs were dispersed in water solution from 6.0 to ~ 4.5 seems to support this hypothesis.

3.2 Colloidal stability

Both, particle size and nature of the surface have a major impact on the interaction of MIL-100 NPs with the biological structures, conditioning their physiological colloidal stability, cell uptake, biodistribution or toxicity, among others. For better understanding the NP-cell interactions, the colloidal stability of MIL-100(Fe, Al, Cr) NPs was assessed by monitoring

the NP size and surface charge over time under the conditions used for the culture of the selected cells (FBS-supplemented-DMEM and -MEM, at 37 °C; Figure 2).

On the whole, the initial particle size of MIL-100(Fe, Al, Cr) NPs in the cell culture media was similar than in pure water with polydispersity values ~ 0.3 (252 \pm 32 vs. 255 \pm 21 nm; 311 \pm 35 vs. 291 \pm 24 nm and 146 \pm 32 vs. 153 \pm 49 nm for Fe-, Al- and Cr-based MIL-100 NPs, respectively) (Table 1 and Figure 2). In addition, ζ -potential values of around -10 mV in the cell culture media for all the MIL-100(Fe, Al, Cr) NPs suggests de formation of a protein corona on the external surface of NPs. Previous studies of MIL-100(Fe) NPs in presence of a phosphate buffer (PBS) supplemented with bovine serum albumin (BSA; the most abundant protein within the mammals serum) already displayed an important reduction of the ζ -potential from -31 mV in PBS to -10 mV in BSA-PBS⁵⁹, in agreement with these results.

In addition, despite slight differences on the chemical composition of DMEM and MEM media, the MIL-100 NPs exhibited similar initial particle size and superficial charge regardless the cell culture media, facilitating the direct comparison of cytotoxicity between the different selected cell lines (see below). Except for the MIL-100(Cr) NPs suspended in MEM, the particle size of MIL-100(Fe, Al, Cr) NPs remained constant along the time (up to 48 h). The important colloidal stability of these NPs in the cell culture media could be explained by the presence of the protein corona by avoiding the interparticle attraction through the introduction of new steric hindrance repulsions⁵⁹. In contrast, although the particle size of MIL-100(Cr) NPs in MEM medium did not significantly change up to 24 h, at 48 h it increased from 153 \pm 4 to 274 \pm 39 nm. This aggregation phenomenon could be explained by the progressive decrease of the absolute superficial charge, from around -10 to -4 mV. One could tentatively attribute the ζ -potential modification to the replacement of the protein by other components of the medium. Additionally, this effect of the neutralization of the surface charge is also observed when the MIL-100(Cr) NPs were suspended for 48 h in DMEM, reaching ζ -potential values similar to MIL-100(Cr) NPs in MEM after 24 h (-6.0 mV). Note here that at this value, MIL-100(Cr) NPs seem to be colloidally stable.

Therefore, for further comparisons of potential cytotoxic effects of MIL-100 NPs, one can conclude that MIL-100(Fe) and (Al) NPs exhibit a similar particle size (230 \pm 22 and 320 \pm 36 nm, respectively) and ζ -potential (*ca.* -10 mV) with a suitable colloidal stability in both DMEM and MEM culture media up to 48 h. The MIL-100(Cr) NPs show smaller dimensions (146 \pm 17nm) and good colloidal stability up to 24 h regardless the culture media, with

however a significant aggregation effect at 48 h in MEM medium, associated to a decrease of the absolute ζ -potential value (from -10 to -4 mV).

3.3 Chemical stability.

A crucial point to take into account for a successful and prolonged drug delivery is the provision of chemical stability to the nanocarrier in biological environment. These nanosystems must be stable in the desired physiological media for an extended period of time in order to reach the target, without compromising the cell viability. In this sense, the chemical stability of MIL-100(Fe, Al, Cr) NPs has been investigated in both cell culture media by assessing the leaching of the constitutive organic linker (trimesic acid) by high-performance liquid chromatography (HPLC) (Figure 3).

Interestingly, with the exception of the MIL-100(Al) NPs in MEM, all the NPs show an important stability in the cell culture media with low degradations (< 6% after 48 h of exposition). In particular, less than 1% degradation was detected for the MIL-100(Cr) NPs after a contact time of 48 h in both media, in agreement with the slower exchange constant rate of the chromium ion (see rate constant for the exchange of a coordinated water molecule of the first coordination shell of a given metal ion of $[M(H_2O)_6]^{3+} = 10^0, 10^{-2}$ and 10^{-6} , for M = Al, Fe, Cr) ⁶⁴. In contrast, the degradation profile of MIL-100(Al) NPs in MEM reached almost 80% at 48 h. Considering the considerably higher stability of these NPs in DMEM (~ 6% degradation), this dramatic instability in MEM might be related with the medium composition. Indeed, MEM comprises a different zwitterionic organic buffering agent (4-(2-hydroxyethyl)-1-piperazineethanesulfonic acid or HEPES), as well as sodium pyruvate and additional non-essential amino acids in comparison with DMEM. The presence of highly complexant groups in the chemical structure of HEPES (sulfate, heterocyclic nitrogen, hydroxyl) and sodium pyruvate (carboxylate), able to compete by the cation coordination with the constitutive metal, could partially explain the lower stability of MIL-100(Al) NPs in MEM. Despite the MEM composition, the iron and chromium based MIL-100 NPs were chemically stable in this medium for 48 h due probably to their slower exchange constant rates ⁶⁴.

Thus, with the exception of the MIL-100(Al) NPs in MEM medium, the rest of the NPs present an important stability under the conditions used for the cytotoxicity assays.

3.4 *In vitro* biocompatibility of MIL-100(Fe, Al, Cr) NPs: Real-time follow-up of cellular impedance

The *in vitro* toxicity of MIL-100(Fe, Al, Cr) NPs on cell growth and proliferation/viability and support adherence was measured by performing a real-time monitoring of cell impedance using the xCELLigence[®] system (ACEA Biosciences, San Diego, CA), which is a powerful and sensitive high-throughput method for the real time simultaneous screening of several cell lines at different concentrations⁵⁹, without any interaction between NPs and the signal³⁷. The four selected cell lines (A549, Calu- 3, HepG2 and Hep3B) were exposed for 72 h to different concentrations of MIL-100(Fe, Al Cr) NPs (6, 32 and 64 $\mu\text{g}\cdot\text{cm}^{-2}$, corresponding to 10, 50 and 100 μg of NPs *per* mL; Figure 4). Note that the expression of doses in $\mu\text{g}\cdot\text{cm}^{-2}$ was chosen to get a more accurate comparison between cell lines and all experiments performed in this study. Thus, after exposure, the variation of cellular impedance was measured by the Cellular Index (CI), an arbitrary unit that integrates possible variations in cellular morphology, viability and proliferation. Except for the Hep3B cell line, no significant differences of the CI values were observed after the exposure to MIL-100(Fe, Al, Cr) NP in comparison to unexposed control cells. These results are in agreement with the absence of severe cytotoxicity of the MIL-100, whatever the metal (Fe, Al, Cr)³⁷. In contrast, the CI of Hep3B cell line significantly decreased after exposure to all MIL-100(Fe, Al, Cr) NPs, notably for the MIL-100(Fe) NPs. Contrary to the *a priori* higher toxicity of chromium based compounds, the cytotoxicity of MIL-100(Fe, Al, Cr) seems to be independent on the nature of the cation^{65, 66}. Moreover, one could rule out the influence of particle size or surface charge on the toxic effect since after the formation of the protein corona in contact with biological media very similar values were observed for all the nanoMOFs. Therefore, the specific cytotoxicity of Hep3B cell line does not come from the culture media or degradation kinetics of the MIL-100 NPs since, except for A549 which was cultivated in DMEM, the other three cell lines were cultivated in MEM medium. In this sense, the important degradation of the MIL-100(Al) NPs in MEM (~80% of degradation after 48 h; Figure 3), leading to a high aluminum leaching (~26.2 $\mu\text{g}\cdot\text{mL}^{-1}$ or 16.7 $\mu\text{g}\cdot\text{cm}^{-2}$), does not induce cytotoxicity in Calu-3 and HepG2 cell lines, ruling out the influence of the leaching of the metal and organic linker on the cytotoxic effect of MIL-100 NPs. Thus, the higher toxicity of the Hep3B cell line in comparison with the rest of cells might be related with intrinsic properties. Indeed, as previously mentioned, the absence of p53 expression in Hep3B cells, acting an essential repairing of the genome integrity, could explain the higher toxicity of MIL-100(Fe, Al, Cr) NPs on these cells.

In any case, since modification of CI integrates different possible cell perturbation, further experiments were conducted for measuring cell death, cell cycle, oxidative stress and genotoxicity. Considering the progressive degradation of the MIL-100 NPs under physiological conditions^{50, 51, 60}, and based on the degradation profiles (Figure 3) shorter exposure times (up to 24 h) were selected for all the following experiments in order to take into account mostly the primary effects induced by the "entire" MILs NPs and not by the degradation products.

3.5 Cell viability

As CI integrates different cell parameters such as viability, morphology and membrane potentials, the cell viability was also measured by flow cytometry after ToPro-3 cell exposure, which permits to discriminate alive from dead cells since this dye incorporates into DNA of dead cells⁶¹. Cells were analyzed after 2 and 24 h of contact time at two doses (6 and 64 $\mu\text{g}\cdot\text{cm}^{-2}$) of MIL-100(Al, Fe, Cr) NPs (Figure 5). Aminated polystyrene nanobeads (PSB-NH₂) were chosen as cell death positive control since they have been recently identified as one of four nanomaterials with an important acute toxicity profile⁶⁷, associated to cell membrane damage⁶⁸ and activation of inflammasome pathway⁶⁹. While PSB-NH₂ effectively induced significant cytotoxicity on A549, Calu-3 and HepG2 lines (up to 100% of cell death) after 24 h of exposure, the highest concentration (64 $\mu\text{g}\cdot\text{cm}^{-2}$) of MIL-100(Al, Fe, Cr) NPs did not induce any significant cytotoxic effect neither at 2 nor 24 h of incubation, in agreement with the absence of significant cytotoxicity observed by xCELLigence technique (Figure 4). In contrast, a significant increase of Hep3B cell death (15 and 39% at 2 and 24 h, respectively) was observed after exposure at the higher concentration (64 $\mu\text{g}\cdot\text{cm}^{-2}$) of MIL-100(Fe) NPs. Once again, these results are in accordance with the data obtained by xCELLigence (Figure 4), indicating a toxicity associated to the iron based NPs. Taking into account that no significant toxicity was detected for neither the MIL-100(Al) or (Cr) NPs, the lower viability observed in MIL-100(Fe) might be related with the iron cation either within the particle or released to the medium (~ 6% of degradation corresponding to 2.0 $\mu\text{g}\cdot\text{mL}^{-1}$ or 1.2 $\mu\text{g}\cdot\text{cm}^{-2}$ of metal).

3.6 Cell internalization of MIL-100 NPs

To fully interpret cytotoxicity data, specifically in absence of cellular effects, it is important to analyze the cellular internalization of MIL-100 NPs⁷⁰. In addition, the cell uptake of the MIL-100(Fe) drug nanocarrier is crucial to deliver their active cargo.⁷¹ Thus, the

interaction/internalization between cells and MIL-100(Fe, Al, Cr) NPs was firstly studied by flow cytometry in terms of modification of the cell granularity through the measurement of side scatter parameter (SSC) (Figure 6 and S1), as previously described for other nanoparticulate systems such as WC-Co and TiO₂ NPs^{61, 62, 72}. Two concentrations of MIL-100(Fe, Al, Cr) NPs (6 and 64 $\mu\text{g}\cdot\text{cm}^{-2}$) were incubated with the A549, Calu-3, Hep3B and HepG2 cell lines for 2 and 24 h. It should be mentioned the significant SCC increase observed after exposure of Hep3B cells at the higher dose of MIL-100 NPs (Figure 6), which may indicate an important cell uptake of MIL-100 NPs, in accordance with previously published MIL-100(Fe) internalization onto fetal cervical carcinoma HeLa or mice macrophages J774 cell lines using confocal microscopy³⁷. Indeed, such a comparison gives only a tendency since confocal microscopy is not a quantitative method, cell lines are quite different and macrophages are specifically in charge of detoxification. However, the cell granulometry did not significantly change upon the MIL-100(Fe, Al, Cr) NPs incubation with A549, Calu-3 and HepG2 cell lines (Figure 6), indicating that either NPs are not in interaction/internalized or that SSC is not well-adapted to assess the MIL-100 NPs uptake (as it is the case for other NPs, such as SiO₂)⁷³.

To elucidate if MIL-100(Fe, Al, Cr) NPs entered into these cells, we exposed Calu-3 cells to the MIL-100(Fe) NPs advantageously labelled with the fluorophore furazan (see Experimental section) to track the particles by both flow cytometry and video-confocal microscopy. Note that this polar fluorophore (i) is strongly associated to the MIL-100(Fe) NPs, being almost no released from NPs to the culture media, and (ii) is not able to penetrate into the cells, as recently published^{14, 37}. Calu-3 cell line was chosen to more precisely explore the MIL-100(Fe) uptake since its cell granulometry upon the contact with the NPs is strictly comparable to that of control cells, suggesting the absence of any NPs cell interaction/uptake (Figure 6). As seen in Figure 6, a rapid (almost immediate) concentration-dependent penetration of MIL-100(Fe) NPs into the Calu-3 cells was observed both by flow cytometry and confocal microscopy. The cell internalization increased as the time in all the tested cell lines, being more important in the A549 and Hep3B lines. Although the specific mechanism of internalization of nanoMOFs is still not known, one could rationally suggest a cell internalization by phagocytosis (without specifying a specific mechanism) considering the particle size of the considered MIL-100(Fe, Al, Cr) NPs^{74, 75}. As larger particle size usually improves the phagocytosis process, one could suggest a progressive cell uptake due to particle aggregation. Note however that here the increase of the cell uptake at 24 h is not

related with a particle aggregation since we have previously evidenced an appropriate colloidal stability for 24 h.

Finally, considering the less favorable case of Calu-3 cells and the similarities between the three MIL-100(Fe, Al, Cr) NPs in terms of ζ -potential and particle size in the cell culture media, one could extrapolate that, even if the SSC is not significantly increased as compared to control cells (Figure 6), MIL-100(Fe, Al, Cr) NPs are internalized by the A549, Calu-3 and HepG2 cell lines.

3.7 Oxidative stress: generation of reactive oxygen species (ROS)

Oxidative stress is often related with NPs cytotoxicity^{76, 77}. Moreover, ROS quantification following exposure is of great interest, especially in the case of metal-based NPs that could induce oxidative stress and cytotoxicity. Despite the absence of toxicity for A549, Calu-3 and HepG2 cell lines, oxidative stress was analyzed after exposure of the 4 cell lines with MIL100(Fe, Al, Cr) NPs. ROS production was monitored using the H₂DCFDA-CM probe (see experimental section), which is firstly internalized within the cells in its reduced state. This reduced form may be then oxidized in presence of different oxygen species into a detectable and quantifiable fluorescent form. The level of intracellular oxidative stress is proportional to the fluorescence intensity. Hydrogen peroxide (H₂O₂) was used as positive control (6.6 mM). To ensure that MIL-100 NPs themselves did not induce any effect on the collected signal, a negative control was systematically performed at the highest concentration (64 $\mu\text{g}\cdot\text{cm}^{-2}$) in absence of H₂DCFDA-CM probe (not shown). No significant ROS production was induced after 2 h of incubation with MIL-100(Al, Fe, Cr) NPs, as compared to the control group, with the exception of Hep3B cells exposed to the highest concentration of MIL100(Fe) NPs (Figure 7). In this case, a significant increase of ROS after 2 h of exposure, up to 1.8 fold the basal level, was evidenced, pointing out the putative role of the oxidative stress generated by the MIL-100(Fe) NPs on the Hep3B cells. This ROS production might be associated with the redox character of iron in comparison with either chromium or aluminum (see spontaneous standard potential E^0 (volts) $\text{Fe}^{3+}(\text{aq}) + \text{e}^- \rightarrow \text{Fe}^{2+}(\text{aq}) = 0.77$ in comparison with negative non-spontaneous processes in Al^{3+} or Cr^{3+}). It is well-known that iron is able to promote the generation of hydroxyl radicals or other reactive species (Haber-Weiss and Fenton's reaction)⁷⁸⁻⁸⁰. Therefore, ROS induction could be related with either the reduction of the iron present within the framework (on the internal and outer surface), or with the free iron coming from the MOF degradation.

The ROS production generated by the MIL-100(Fe) NPs is however strongly dependent both on the cell line and on the time/concentration. Bearing in mind the influence of the cell line on the ROS, except for the Hep3B cells, the rest of the tested cells (A549, Calu-3 and HepG2) did not exhibit any ROS induction. This is in agreement with the more sensitive character of the Hep3B line. In this sense, some of us have recently evidenced a significant increase of the ROS upon the exposure of human promyelocytic leukemia HL-60 cell line to $250 \mu\text{g.mL}^{-1}$ of MIL-100(Fe) NPs ⁸¹.

Considering the influence of the time and concentration, only high doses led to ROS induction ($100 \text{ vs. } 10 \mu\text{g.mL}^{-1}$), in accordance with recent results obtained with HL-60 cells ($250 \text{ vs. } 25 \mu\text{g.mL}^{-1}$). It is noteworthy that no oxidative stress was detected at longer times (24 h), indicating a transient oxidative effect, in agreement with the reversible increase of the oxidative stress, previously evidenced after the intravenous administration of high doses of MIL-100(Fe) NPs to rats ²⁶. Longer contact times can be associated *in vitro* to higher ROS production depending on the cell line and nanoMOF doses (no ROS at ≤ 8 h while ROS production at 24 h in HL-60) ⁸¹.

3.8 Cell cycle analysis

The cell cycle, almost no studied in MOFs, is an important parameter to point out since, even without direct induced cytotoxicity, the proliferative capacity of the cells can be disturbed indicating cell damages. The impact of the three MIL-100 NPs on cell cycle was studied using ToPro3 (TP3) staining by flow cytometry using FlowJo software (see experimental section). The NPs were incubated at two concentrations (6 and $64 \mu\text{g.cm}^{-2}$) for 2 and 24 h with the four cell lines (Figure 8). PSB-NH₂ NPs have been used as positive control since these NPs induced strong cell cytotoxicity⁸². Remarkably, no significant modification of the cell cycle was noticed in the four tested cell lines exposed to the MIL-100(Fe, Al, Cr) NPs regardless the cation and the cell line.

Thus, the absence of cytotoxicity described previously for A549, Calu-3, HepG2 (MIL-100(Fe, Al, Cr) NPs) and Hep3B (only MIL-100(Al, Cr) NPs) cell lines is confirmed again since no modification of cell proliferation was observed. Concerning the more sensitive Hep3B cells exposed to the highest dose ($64 \mu\text{g.cm}^{-2}$) of MIL-100(Fe), the cell cycle remained unchanged, although a transient increase of oxidative stress was observed together with increased mortality. This is reliable with a specificity of this cell line that does not express p53 protein, a major actor for the regulation of the cell cycle after a stress ⁸³.

Normally, in p53 wild type cells after ROS induced DNA damages, this protein arrests cell cycle for proper initiation of DNA repair before any cell division, a crucial point essential for maintaining genome integrity.

Overall, MIL-100(Al, Fe, Cr) NPs do not alter cell cycle of A549, Calu-3, HepG2 and Hep3B cell lines after 2 and 24 h. Indeed, this result was expected after exposure with the MIL-100(Al, Cr) that induce neither cytotoxicity nor ROS, regardless the nature of the metal, particle size or ζ -potential. The absence of cell cycle arrest after exposure of Hep3B cells to the highest dose of MIL-100(Fe), despite de oxidative stress, is related to the absence of P53. It could explain also the observed cytotoxicity assuming that the ROS induced DNA damages in Hep3B cells are not repaired before cell division.

3.9 Genotoxicity: DNA damages

The above experiments have confirmed the absence of toxicity for the MIL-100(Fe, Al, Cr) NPs on the tested cell lines, with the exception of one condition: Hep3B exposed to a high dose MIL-100(Fe) NPs ($64 \mu\text{g}\cdot\text{cm}^{-2}$), where a significant increase of cell death together with a ROS production was observed. Taking into account that the potential genotoxicity of different nanoparticulate systems has been established through oxidative stress⁸⁴, we here studied whether oxidative stress followed by cell death after Hep3B exposure with MIL-100(Fe) NPs could result from DNA damages. Thus, DNA strand breaks were quantified by labeling the Ser129 phosphorylation of histone variant H2AX. The phosphorylation of this histone, which is specifically recruited at the sites rounding double strand breaks, is considered to be the most sensitive method for monitoring DNA damages⁸⁵ as well as a powerful approach to predict *in vivo* genotoxicity⁸⁶. Note here that, to the best of our knowledge, no genotoxicity studies dealing with nanoMOFs have been reported so far. Thus, Figure 9 shows the results obtained for Hep3B exposed for 24 h to MIL-100(Fe, Al, Cr) NPs at two doses (6 and $64 \mu\text{g}\cdot\text{cm}^{-2}$). No significant increase of the number of γ -H2Ax *foci per nuclei* was observed, except for MIL-100(Fe) at the highest concentration ($64 \mu\text{g}\cdot\text{cm}^{-2}$), in which the median comes from 3 to 5 *foci per nuclei* ($0.001 < p < 0.05$). Considering that these cells lack p53 (contrary to HepG2 cell line) and that only one DNA double strand break may be fatal for cell integrity, this relatively low level of DNA damages should be related with the observed ROS increase and, therefore, to subsequent cell death induced by MIL-100(Fe) at the highest concentration. These results are also consistent with the xCELLigence curves, where CI is diminished in a concentration dependent way (Figure 4).

4. Conclusion

Based on the high potential industrial and societal interest of MIL-100 solids, the aim of this study was to determine and understand the toxicity of the Fe, Al and Cr-based MIL-100 NPs. To ensure safety prior to any applications, we addressed the question of the influence of the metal to trigger different cellular response using four human cell lines. Considering a pulmonary, ingestion or intravenous exposure mode, two pulmonary and two hepatic cell lines were basically selected.

Despite the initial significantly different particle size and ζ -potential of the NPs, physicochemical characterization in the physiological media (the used cell culture media: DMEM and MEM) evidenced (i) a similar superficial charge and particle size, except for the smaller dimensions of MIL-100(Cr) NPs, (ii) an high colloidal stability from 24 to 48 h and (iii) an important chemical stability, with very low degradation rates, except for the MIL-100(Al) NPs exclusively in contact with the MEM medium.

By measuring cell impedance, cell survival/death, ROS generation and the level of DNA damage, we found that MIL-100(Fe, Al, Cr) NPs do not induce *in vitro* cell toxicity, even at high doses in the p53 wild type cell lines (A 549 and Calu-3 (lung) and HepG2 (liver)). The only toxic effect of MIL-100(Fe) NPs was observed in the hepatocarcinoma cell line Hep3B, which is highly sensitive due to its absence of TP53 expression, the guardian of the genome. However, even if adverse effects are detected in the most sensitive cell line Hep3B, it has to be balanced with three major facts: (1) the doses that will be used for medical applications will be greatly lower than those used in this study, (2) for drug delivery in pathologies others than cancer, cells will be p53 wild type like A549, Calu-3 and HepG2, (3) in dynamic conditions, such as a living being, the progressively degraded MIL-100(Fe) NPs will be excreted, thus limiting an accumulation, as previously described⁵¹. These data also indicate that for cancer drug delivery, since numerous tumors are mutated for p53, the MIL-100(Fe) NPs drug carriers could be more efficient for inducing cell death (as compared to drug alone).

These original data confirm that MIL-100 NPs are able to enter into the cells. The possibility of controlling the drug concentrations parameters allows following future experiments based on the drug containing MIL-100(Fe) NPs to target diseases through NPs inhalation, intravenous or ingestion.

Altogether, our data point out a high cell tolerance for MIL-100(Fe, Al, Cr) NPs that should be further documented by *in vivo* studies before their use in the biomedical field or other important industrial fields.

Acknowledgements

The authors declare no competing conflict of interests.

This work was funded by the NanoSciences and Technology pour la Santé CEA-Transverse program, the Dim C’Nano IdF, the EU Framework 7 Program NANOREG 1 and the French Agency for Food, Environmental and Occupational Health Safety (ANSES). RG is a recipient of a fellowship from ANSES.

References

1. H. C. Zhou and S. Kitagawa, *Chemical Society reviews*, 2014, **43**, 5415-5418.
2. S. Qiu, M. Xue and G. Zhu, *Chemical Society reviews*, 2014, **43**, 6116-6140.
3. J. Liu, L. Chen, H. Cui, J. Zhang, L. Zhang and C. Y. Su, *Chemical Society reviews*, 2014, **43**, 6011-6061.
4. Z. Hu, B. J. Deibert and J. Li, *Chemical Society reviews*, 2014, **43**, 5815-5840.
5. P. Horcajada, R. Gref, T. Baati, P. K. Allan, G. Maurin, P. Couvreur, G. Ferey, R. E. Morris and C. Serre, *Chemical reviews*, 2012, **112**, 1232-1268.
6. Y. Cui, Y. Yue, G. Qian and B. Chen, *Chemical reviews*, 2012, **112**, 1126-1162.
7. S. R. Meyers and M. W. Grinstaff, *Chemical reviews*, 2012, **112**, 1615-1632.
8. T. H. Tran-Thi, R. Dagnelie, S. Crunaire and L. Nicole, *Chemical Society reviews*, 2011, **40**, 621-639.
9. J. Rocha, L. D. Carlos, F. A. Paz and D. Ananias, *Chemical Society reviews*, 2011, **40**, 926-940.
10. M. D. Allendorf, C. A. Bauer, R. K. Bhakta and R. J. Houk, *Chemical Society reviews*, 2009, **38**, 1330-1352.
11. J. Lee, O. K. Farha, J. Roberts, K. A. Scheidt, S. T. Nguyen and J. T. Hupp, *Chemical Society reviews*, 2009, **38**, 1450-1459.
12. J. Della Rocca, D. Liu and W. Lin, *Accounts of chemical research*, 2011, **44**, 957-968.
13. I. Imaz, M. Rubio-Martinez, J. An, I. Sole-Font, N. L. Rosi and D. Maspoch, *Chemical communications*, 2011, **47**, 7287-7302.
14. C. Tamames-Tabar, A. García-Márquez, M. J. Blanco-Prieto, C. Serre and P. Horcajada, in *Bio- and Bioinspired Nanomaterials*, Wiley-VCH Verlag GmbH & Co. KGaA, 2014, DOI: 10.1002/9783527675821.ch04, pp. 83-112.
15. C. He, K. Lu, D. Liu and W. Lin, *Journal of the American Chemical Society*, 2014, **136**, 5181-5184.
16. W. Morris, W. E. Briley, E. Auyeung, M. D. Cabezas and C. A. Mirkin, *Journal of the American Chemical Society*, 2014, **136**, 7261-7264.
17. A. Wicki, D. Witzigmann, V. Balasubramanian and J. Huwyler, *Journal of controlled release : official journal of the Controlled Release Society*, 2015, **200**, 138-157.
18. S. Ramishetti and L. Huang, *Therapeutic delivery*, 2012, **3**, 1429-1445.
19. J. H. Adair, M. P. Parette, E. I. Altinoglu and M. Kester, *ACS nano*, 2010, **4**, 4967-4970.

20. P. P. Adisheshaiah, J. B. Hall and S. E. McNeil, *Wiley interdisciplinary reviews. Nanomedicine and nanobiotechnology*, 2010, **2**, 99-112.
21. Y. Diebold and M. Calonge, *Progress in retinal and eye research*, 2010, **29**, 596-609.
22. E. Fattal and Tsapis, *Clinical Translational Imaging*, 2014.
23. M. Ferrari, *Nature reviews. Cancer*, 2005, **5**, 161-171.
24. V. Weissig, T. K. Pettinger and N. Murdock, *International journal of nanomedicine*, 2014, **9**, 4357-4373.
25. Regulation, (EC), No, 1907/2006; O. L, 396, of and 12, 2006.
26. T. Baati, L. Njim, F. Neffati, A. Kerkeni, M. Bouttemi, R. Gref, M. F. Najjar, A. Zakhama, P. Couvreur, C. Serre and P. Horcajada, *Chemical Science*, 2013, **4**, 1597-1607.
27. T. Baati, P. Horcajada, R. Gref, P. Couvreur and C. Serre, *Journal of Pharmaceutical and Biomedical Analysis*, 2011, **56**, 758-762.
28. À. Ruyra, A. Yazdi, J. Espín, A. Carné-Sánchez, N. Roher, J. Lorenzo, I. Imaz and D. Maspoch, *Chemistry – A European Journal*, 2015, **21**, 2508-2518.
29. Q. L. Zhu and Q. Xu, *Chemical Society reviews*, 2014, **43**, 5468-5512.
30. W. Lu, Z. Wei, Z. Y. Gu, T. F. Liu, J. Park, J. Park, J. Tian, M. Zhang, Q. Zhang, T. Gentle, 3rd, M. Bosch and H. C. Zhou, *Chemical Society reviews*, 2014, **43**, 5561-5593.
31. V. Guillermin, D. Kim, J. F. Eubank, R. Luebke, X. Liu, K. Adil, M. S. Lah and M. Eddaoudi, *Chemical Society reviews*, 2014, **43**, 6141-6172.
32. A. Mehdi, C. Reye and R. Corriu, *Chemical Society reviews*, 2011, **40**, 563-574.
33. J. M. Oh, D. H. Park and J. H. Choy, *Chemical Society reviews*, 2011, **40**, 583-595.
34. Z. Wang and S. M. Cohen, *Chemical Society reviews*, 2009, **38**, 1315-1329.
35. T. Chalati, P. Horcajada, P. Couvreur, C. Serre, M. Ben Yahia, G. Maurin and R. Gref, *Nanomedicine*, 2011, **6**, 1683-1695.
36. L. Cooper, T. Hidalgo, M. Gorman, T. Lozano-Fernandez, R. Simon-Vazquez, C. Olivier, N. Guillou, C. Serre, C. Martineau, F. Taulelle, D. Damasceno-Borges, G. Maurin, A. Gonzalez-Fernandez, P. Horcajada and T. Devic, *Chemical communications*, 2015, **51**, 5848-5851.
37. C. Tamames-Tabar, D. Cunha, E. Imbuluzqueta, F. Ragon, C. Serre, M. J. Blanco-Prieto and P. Horcajada, *Journal of Materials Chemistry B*, 2014, **2**, 262-271.
38. P. Horcajada, S. Surble, C. Serre, D. Y. Hong, Y. K. Seo, J. S. Chang, J. M. Greneche, I. Margiolaki and G. Ferey, *Chemical communications*, 2007, DOI: 10.1039/b704325b, 2820-2822.
39. C. Volkringer, D. Popov, T. Loiseau, G. Férey, M. Burghammer, C. Riekel, M. Haouas and F. Taulelle, *Chemistry of Materials*, 2009, **21**, 5695-5697.
40. G. Ferey, C. Serre, C. Mellot-Draznieks, F. Millange, S. Surble, J. Dutour and I. Margiolaki, *Angewandte Chemie*, 2004, **43**, 6296-6301.
41. A. Lieb, H. Leclerc, T. Devic, C. Serre, I. Margiolaki, F. Mahjoubi, J. S. Lee, A. Vimont, M. Daturi and J.-S. Chang, *Microporous and Mesoporous Materials*, 2012, **157**, 18-23.
42. J. P. S. Mowat, S. R. Miller, A. M. Z. Slawin, V. R. Seymour, S. E. Ashbrook and P. A. Wright, *Microporous and Mesoporous Materials*, 2011, **142**, 322-333.
43. Y. K. Park, S. B. Choi, H. Kim, K. Kim, B. H. Won, K. Choi, J. S. Choi, W. S. Ahn, N. Won, S. Kim, D. H. Jung, S. H. Choi, G. H. Kim, S. S. Cha, Y. H. Jhon, J. K. Yang and J. Kim, *Angewandte Chemie*, 2007, **46**, 8230-8233.
44. A. Vimont, J. M. Goupil, J. C. Lavalley, M. Daturi, S. Surble, C. Serre, F. Millange, G. Ferey and N. Audebrand, *Journal of the American Chemical Society*, 2006, **128**, 3218-3227.
45. J. W. Yoon, Y. K. Seo, Y. K. Hwang, J. S. Chang, H. Leclerc, S. Wuttke, P. Bazin, A. Vimont, M. Daturi, E. Bloch, P. L. Llewellyn, C. Serre, P. Horcajada, J. M. Greneche, A. E. Rodrigues and G. Ferey, *Angewandte Chemie*, 2010, **49**, 5949-5952.
46. P. L. Llewellyn, S. Bourrelly, C. Serre, A. Vimont, M. Daturi, L. Hamon, G. De Weireld, J. S. Chang, D. Y. Hong, Y. Kyu Hwang, S. Hwa Jhung and G. Ferey, *Langmuir : the ACS journal of surfaces and colloids*, 2008, **24**, 7245-7250.

47. M. Latroche, S. Surble, C. Serre, C. Mellot-Draznieks, P. L. Llewellyn, J. H. Lee, J. S. Chang, S. H. Jung and G. Ferey, *Angewandte Chemie*, 2006, **45**, 8227-8231.
48. Z. Y. Gu and X. P. Yan, *Angewandte Chemie*, 2010, **49**, 1477-1480.
49. M. Maes, M. Trekels, M. Boulhout, S. Schouteden, F. Vermoortele, L. Alaerts, D. Heurtaux, Y. K. Seo, Y. K. Hwang, J. S. Chang, I. Beurroies, R. Denoyel, K. Temst, A. Vantomme, P. Horcajada, C. Serre and D. E. De Vos, *Angewandte Chemie*, 2011, **50**, 4210-4214.
50. Y. K. Seo, J. W. Yoon, J. S. Lee, Y. K. Hwang, C. H. Jun, J. S. Chang, S. Wuttke, P. Bazin, A. Vimont, M. Daturi, S. Bourrelly, P. L. Llewellyn, P. Horcajada, C. Serre and G. Ferey, *Advanced materials*, 2012, **24**, 806-810.
51. P. Horcajada, T. Chalati, C. Serre, B. Gillet, C. Sebrie, T. Baati, J. F. Eubank, D. Heurtaux, P. Clayette, C. Kreuz, J. S. Chang, Y. K. Hwang, V. Marsaud, P. N. Bories, L. Cynober, S. Gil, G. Ferey, P. Couvreur and R. Gref, *Nature materials*, 2010, **9**, 172-178.
52. P. Horcajada, C. Serre, M. Vallet-Regi, M. Sebban, F. Taulelle and G. Ferey, *Angewandte Chemie*, 2006, **45**, 5974-5978.
53. L. L. Brunton, D. K. Blumenthal, I. L. O. Buxton and K. Parker, *Manual of Pharmacology and Therapeutics*, 2008.
54. C. Exley, P. Siesjo and H. Eriksson, *Trends in immunology*, 2010, **31**, 103-109.
55. S. Lu, R. Duffin, C. Poland, P. Daly, F. Murphy, E. Drost, W. Macnee, V. Stone and K. Donaldson, *Environmental health perspectives*, 2009, **117**, 241-247.
56. J. I. Mujika, F. Ruiperez, I. Infante, J. M. Ugalde, C. Exley and X. Lopez, *The journal of physical chemistry. A*, 2011, **115**, 6717-6723.
57. J. C. Rutherford and A. J. Bird, *Eukaryotic cell*, 2004, **3**, 1-13.
58. A. García Márquez, A. Demessence, A. E. Platero-Prats, D. Heurtaux, P. Horcajada, C. Serre, J.-S. Chang, G. Férey, V. A. de la Peña-O'Shea, C. Boissière, D. Grosso and C. Sanchez, *European Journal of Inorganic Chemistry*, 2012, **2012**, 5165-5174.
59. E. Bellido, M. Guillevic, T. Hidalgo, M. J. Santander-Ortega, C. Serre and P. Horcajada, *Langmuir : the ACS journal of surfaces and colloids*, 2014, **30**, 5911-5920.
60. D. Cunha, M. Ben Yahia, S. Hall, S. R. Miller, H. Chevreau, E. Elkaïm, G. Maurin, P. Horcajada and C. Serre, *Chemistry of Materials*, 2013, **25**, 2767-2776.
61. V. Paget, J. A. Sergent, R. Grall, S. Altmeyer-Morel, H. A. Girard, T. Petit, C. Gesset, M. Mermoux, P. Bergonzo, J. C. Arnault and S. Chevillard, *Nanotoxicology*, 2014, **8 Suppl 1**, 46-56.
62. R. M. Zucker, E. J. Massaro, K. M. Sanders, L. L. Degn and W. K. Boyes, *Cytometry. Part A : the journal of the International Society for Analytical Cytology*, 2010, **77**, 677-685.
63. R. Nunez, *Current issues in molecular biology*, 2001, **3**, 67-70.
64. L. Helm and A. E. Merbach, *Chemical reviews*, 2005, **105**, 1923-1959.
65. D. Beyersmann and A. Hartwig, *Archives of toxicology*, 2008, **82**, 493-512.
66. D. Bagchi, M. Bagchi and S. J. Stohs, *Molecular and cellular biochemistry*, 2001, **222**, 149-158.
67. X. Z. Wang, Y. Yang, R. Li, C. McGuinness, J. Adamson, I. L. Megson and K. Donaldson, *Nanotoxicology*, 2014, **8**, 465-476.
68. P. Ruenaroengsak, P. Novak, D. Berhanu, A. J. Thorley, E. Valsami-Jones, J. Gorelik, Y. E. Korchev and T. D. Tetley, *Nanotoxicology*, 2012, **6**, 94-108.
69. O. Lunov, T. Syrovets, C. Loos, G. U. Nienhaus, V. Mailander, K. Landfester, M. Rouis and T. Simmet, *ACS nano*, 2011, **5**, 9648-9657.
70. E. Frohlich, *International journal of nanomedicine*, 2012, **7**, 5577-5591.
71. B. Yameen, W. I. Choi, C. Vilos, A. Swami, J. Shi and O. C. Farokhzad, *Journal of controlled release : official journal of the Controlled Release Society*, 2014, **190**, 485-499.
72. V. Paget, H. Moche, T. Kortulewski, R. Grall, L. Irbah, F. Nessler and S. Chevillard, *Toxicological sciences : an official journal of the Society of Toxicology*, 2014, DOI: 10.1093/toxsci/kfu238.
73. J. A. Sergent, V. Paget and S. Chevillard, *The Annals of occupational hygiene*, 2012, **56**, 622-630.

74. S. Muro, C. Garnacho, J. A. Champion, J. Leferovich, C. Gajewski, E. H. Schuchman, S. Mitragotri and V. R. Muzykantov, *Molecular therapy : the journal of the American Society of Gene Therapy*, 2008, **16**, 1450-1458.
75. S. E. Gratton, P. A. Ropp, P. D. Pohlhaus, J. C. Luft, V. J. Madden, M. E. Napier and J. M. DeSimone, *Proceedings of the National Academy of Sciences of the United States of America*, 2008, **105**, 11613-11618.
76. S. Hussain, S. Garantziotis, F. Rodrigues-Lima, J. M. Dupret, A. Baeza-Squiban and S. Boland, *Advances in experimental medicine and biology*, 2014, **811**, 111-134.
77. F. Marano, S. Hussain, F. Rodrigues-Lima, A. Baeza-Squiban and S. Boland, *Archives of toxicology*, 2011, **85**, 733-741.
78. F. Haber and J. Weiss, *The Catalytic Decomposition of Hydrogen Peroxide by Iron Salts*, 1934.
79. A. Samuni, M. Chevion and G. Czapski, *The Journal of biological chemistry*, 1981, **256**, 12632-12635.
80. H. J. H. Fenton, *Journal of the Chemical Society, Transactions*, 1894, **65**, 899-910.
81. E. Bellido, T. Hidalgo, M. V. Lozano, M. Guillevic, R. Simon-Vazquez, M. J. Santander-Ortega, A. Gonzalez-Fernandez, C. Serre, M. J. Alonso and P. Horcajada, *Advanced healthcare materials*, 2015, DOI: 10.1002/adhm.201400755.
82. V. Paget, S. Dekali, T. Kortulewski, R. Grall, C. Gamez, K. Blazy, O. Aguerre-Chariol, S. Chevillard, A. Braun, P. Rat and G. Lacroix, *PLoS one*, 2015, **10**, e0123297.
83. N. D. Lakin and S. P. Jackson, *Oncogene*, 1999, **18**, 7644-7655.
84. N. Singh, B. Manshian, G. J. Jenkins, S. M. Griffiths, P. M. Williams, T. G. Maffei, C. J. Wright and S. H. Doak, *Biomaterials*, 2009, **30**, 3891-3914.
85. C. E. Redon, A. J. Nakamura, O. A. Martin, P. R. Parekh, U. S. Weyemi and W. M. Bonner, *Aging*, 2011, **3**, 168-174.
86. D. J. Smart, K. P. Ahmedi, J. S. Harvey and A. M. Lynch, *Mutation research*, 2011, **715**, 25-31.

Table 1. Particle size and ξ -potential of MIL-100(Fe), MIL-100(Al) and MIL-100(Cr) NPs in different media together with their pore surface.

	Medium	MIL-100(Fe)	MIL-100(Al)	MIL-100(Cr)
Size (nm) (Pdl)	H ₂ O	139±25 (0.1)	249±28 (0.2)	142±63 (0.2)
	EtOH	168±10 (0.1)	237±41 (>0.3)	80±41 (0.1)
	DMEM	252±32 (>0.3)	311±41 (>0.3)	146±32 (0.3)
	MEM	255±21 (0.3)	291±24 (>0.3)	153±49 (0.3)
ξ -potential (mV)	H ₂ O	-26±4	+9±1	-15±3
	EtOH	-30±2	+34±7	+32±11
	DMEM	-11±2	-10±1	-10±1
	MEM	-11±1	-12±1	-10±1
BET surface(m ² •g ⁻¹)*		1530	1510	1400

* Brunauer-Emmett-Teller (BET) surface area

Figure 1. XRPD patterns of MIL-100(Fe), MIL-100(Al) and MIL-100(Cr) NPs and TEM images

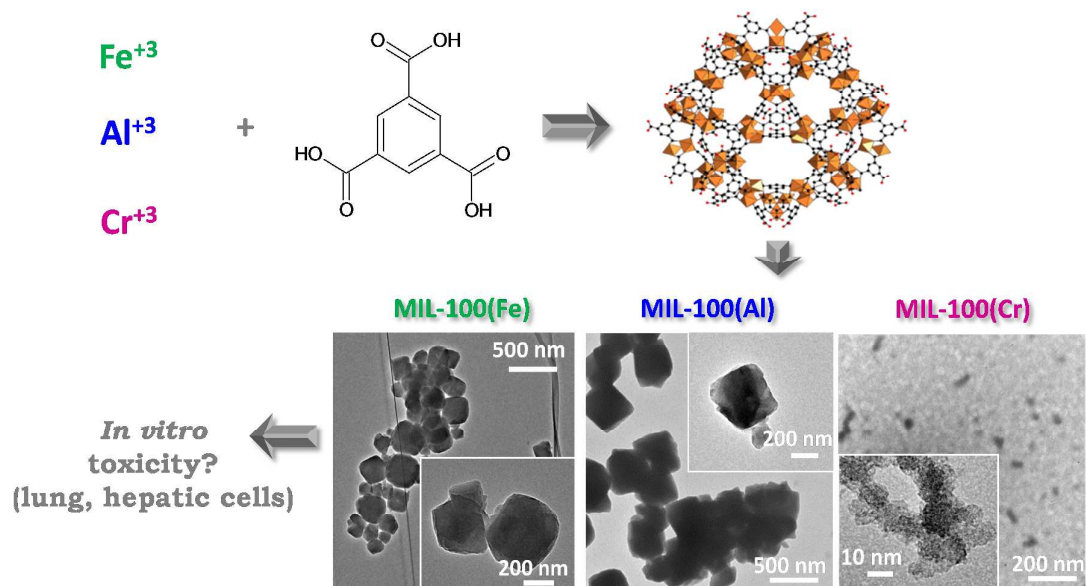


Figure 2. A) Colloidal stability of MIL-100(Fe), MIL-100(Al) and MIL-100(Cr) NPs in cell culture media (DMEM and MEM) at 37 °C. Stability is represented as the average of particle size evolution over time period. B) ζ -potential of MIL-100(Fe), MIL-100(Al) and MIL-100(Cr) NPs in cell culture media as function of time at 37 °C.

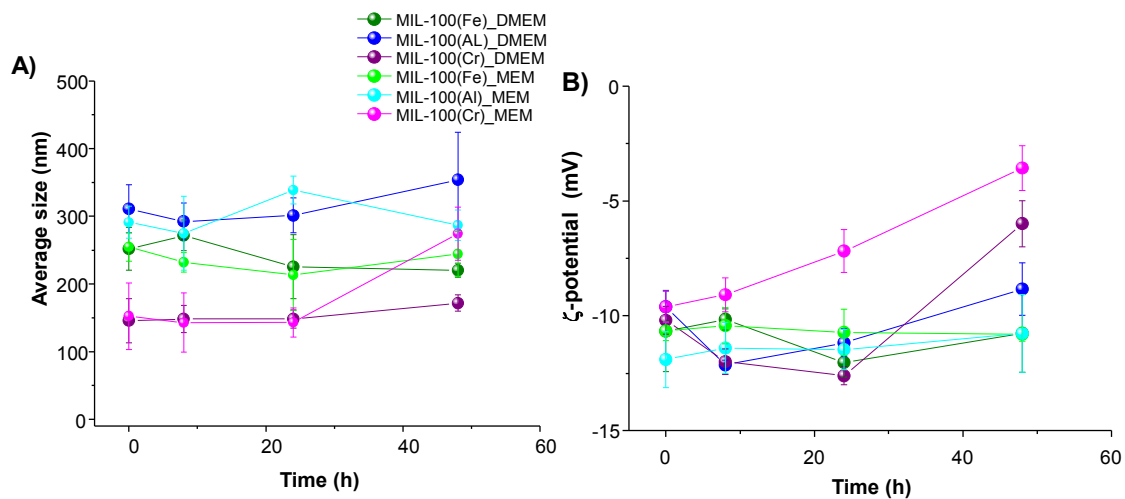


Figure 3. Degradation kinetics of MIL-100(Fe), MIL-100(Al) and MIL-100(Cr) NPs at 37 °C as a function of time in different cell culture media (DMEM and MEM). Degradation is represented as the wt% of the linker released in the medium, considering the maximum of degradation of 100 % when the total amount of linker in the NP is released in the medium.

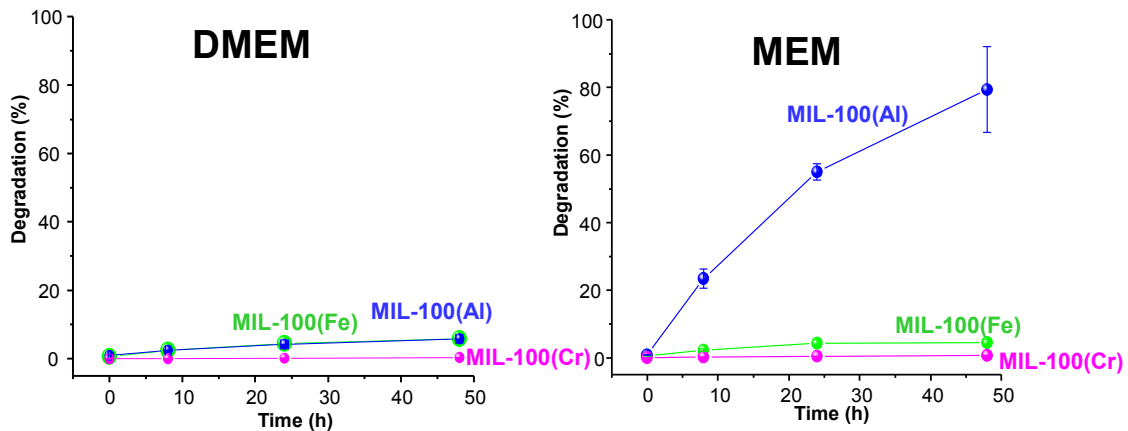


Figure 4. Real-time monitoring of cells exposed to H-NDs and/or irradiation to measure the cell index. Real-time monitoring of the cell index in A549, Calu-3, HepG2 and Hep3B cells exposed to three dose levels of MIL-100(Fe), MIL-100(Al) and MIL-100(Cr) NPs. Impedance measurements (one representative experiment among three independent experiments is shown) were carried out for 80 h and the cell index values were normalized at time 0 to avoid inter-well variability prior to the addition of NPs. “Control” cells were not exposed to MIL-100 NPs.

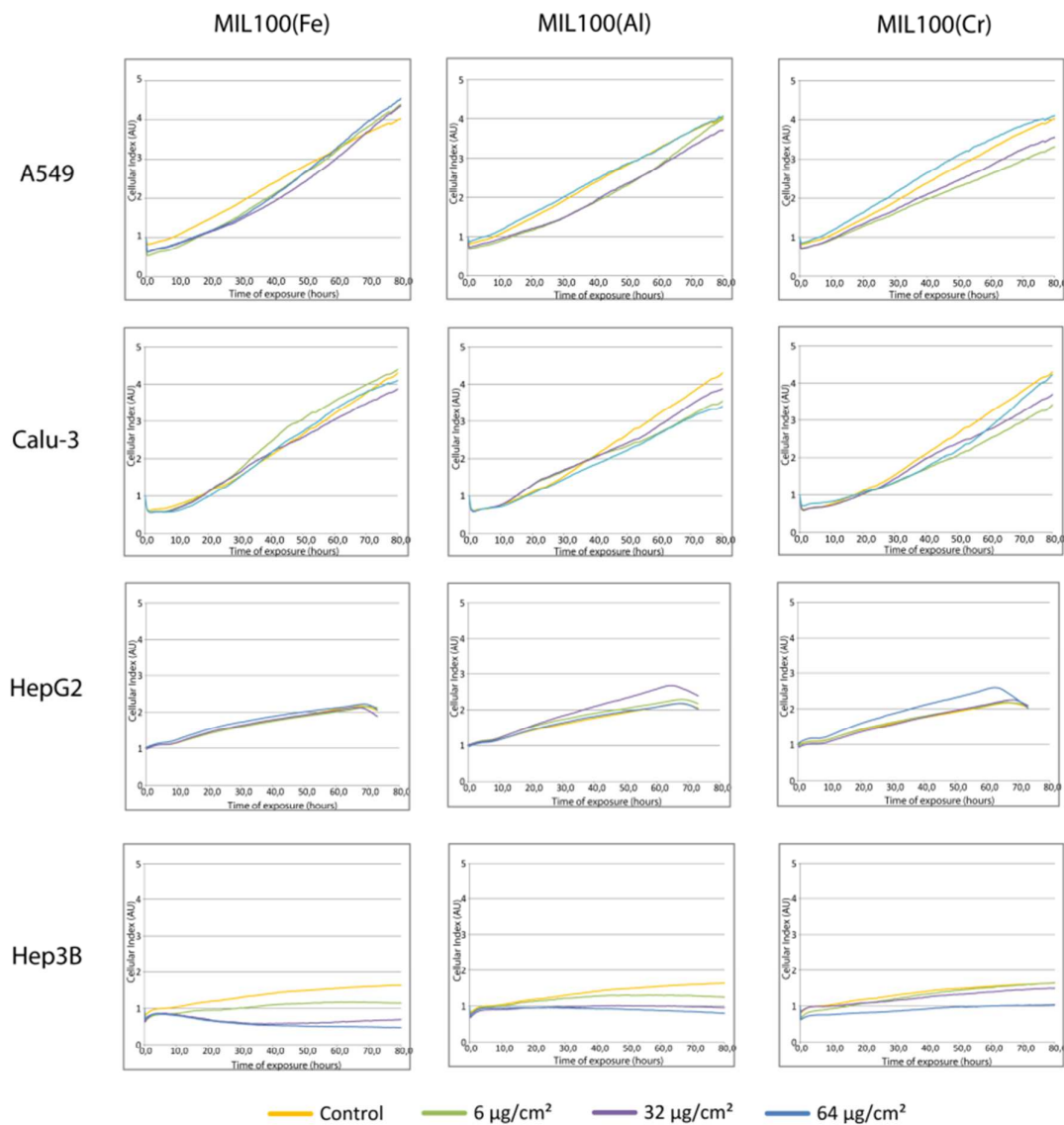


Figure 5. Cell death induction after MIL-100(Fe, Al, Cr) treatments. Cell death measurements of A549, Calu-3, HepG2 and Hep3B cells exposed to 6 and 64 $\mu\text{g}/\text{cm}^2$ of MIL-100 NPs. Cell death induction is represented as the percentage of dead cells among the entire population. Cell counts were taken at 2 and 24 h after treatment. Dead cells labeled by ToPro-3 were counted by flow cytometry (FacsCalibur). “Control” cells were not exposed to MIL-100 NPs. Statistical analysis was performed for each exposure condition compared to non-exposed cells (Student's t-test, * $p < 0.01$).

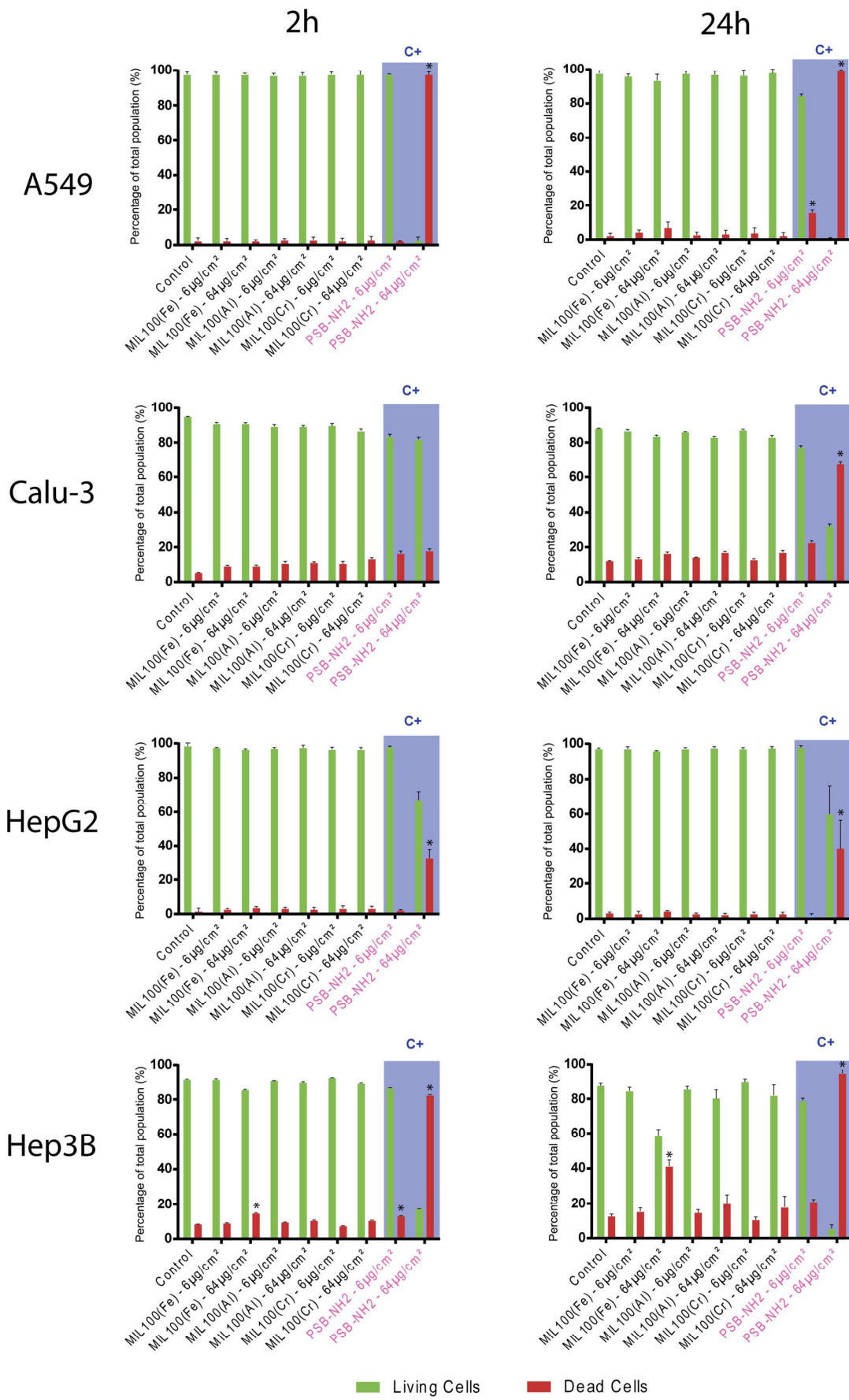


Figure 6. MIL100 internalization into the cells. Flow cytometry analysis of cell granularity by measuring side scatter parameter (SSC) of A549, Calu-3, HepG2 and Hep3B cells exposed to MIL-100(Fe) NPs at two doses (6 and 64 $\mu\text{g}/\text{cm}^2$) for 2 and 24 h.

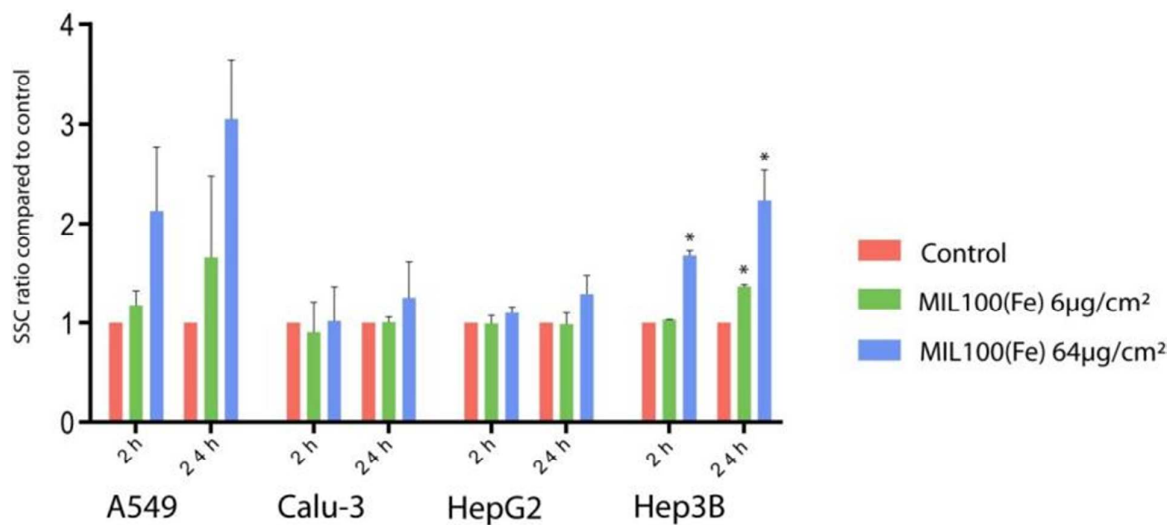


Figure 7. Intracellular generation of reactive oxygen species (ROS) by MIL-100 treatments. A549, Calu-3, HepG2 and Hep3B cells were treated for 2 h with MIL-100(Fe, Al, Cr) NPs (6 and 64 $\mu\text{g}/\text{cm}^2$). Control (basal level) cells were not exposed to MIL-100 NPs. The ROS level was monitored by measurement of the fluorescence intensity of an oxidized fluorescent probe. Ratios as compared to the basal level are here reported. Statistical analysis was performed for each exposure condition compared to non-exposed cells (Student's t-test, * $p < 0.01$).

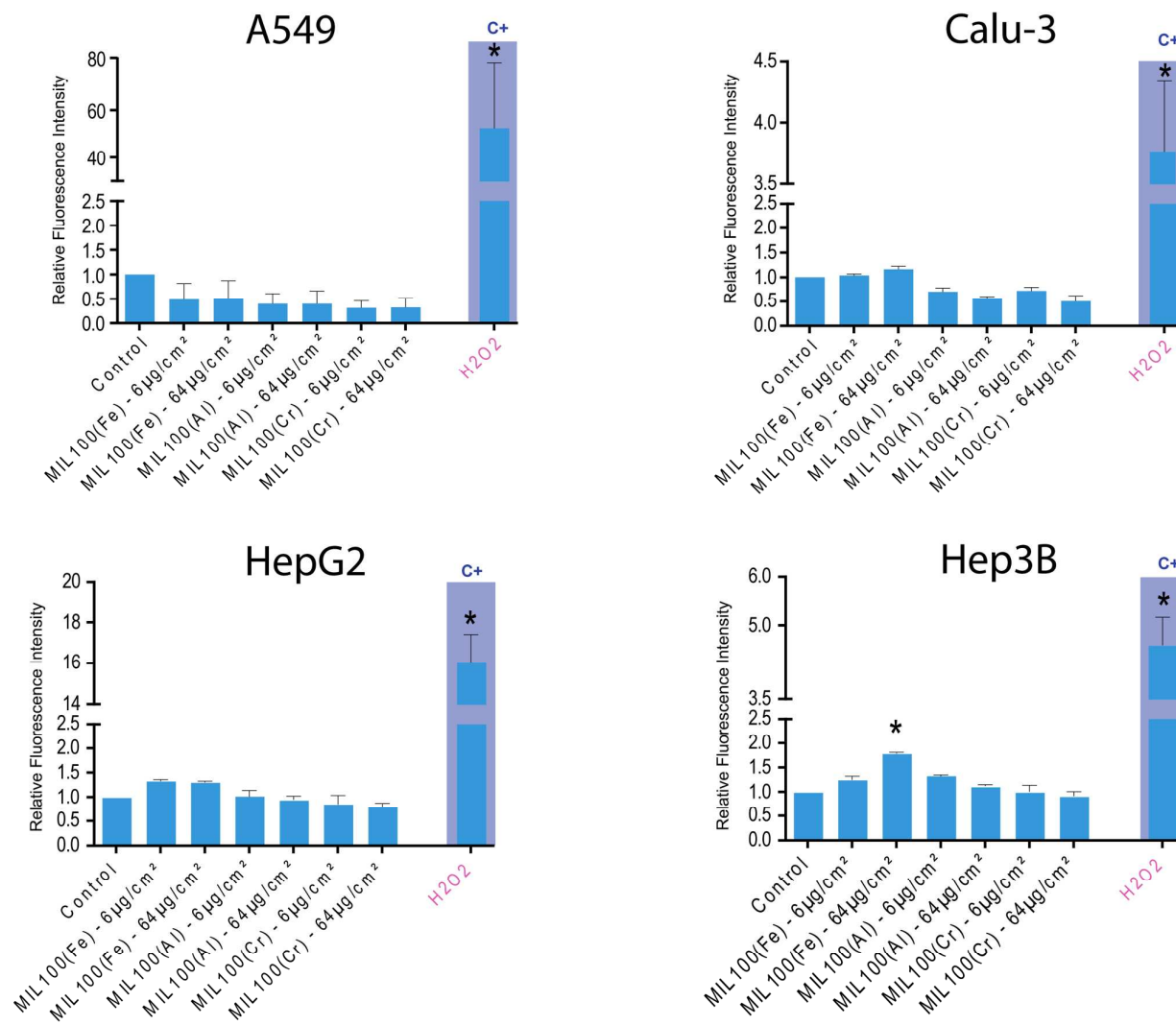


Figure 8. Cell cycle checkpoint activation following MIL100 and/or irradiation treatments. Cell cycle analysis of A549, Calu-3, HepG2 and Hep3B cells exposed to 6 and 64 $\mu\text{g}/\text{cm}^2$ of MIL100. Control cells were not exposed to MIL100. PSB-NH₂ nanobeads were used as been used as positive control. Cell cycle checkpoint activation was evaluated by flow cytometry (FacsCalibur) 2 and 24 h after treatment. Statistical analysis was performed for each exposure condition compared to non-exposed cells (Student's t-test, * $p < 0.01$).

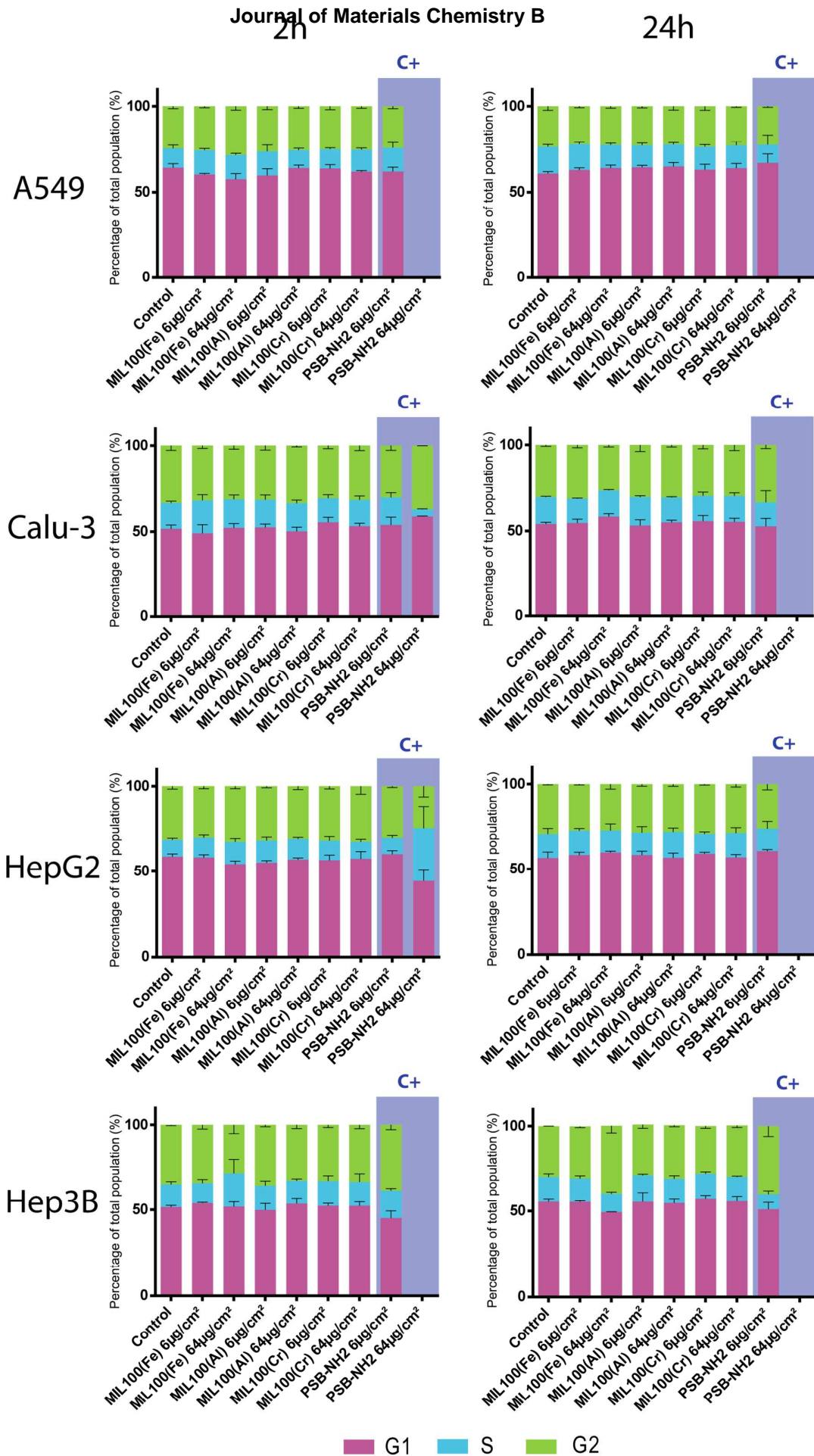


Figure 9. H-ND genotoxicity measured by γ -H2Ax foci counts. γ -H2Ax foci were counted in Hep3B cells exposed to MIL-100(Fe) NPs for 24 h. “Control” cells were not exposed to MIL-100(Fe). Counts were performed on at least 100 cells *per* condition and results are depicted as distribution values of the number of foci obtained for each tested condition (the median is also reported for each sample as well as 25th and 75th percentile and lowest and highest value). A Wilcoxon rank test (comparisons *versus* control cells not exposed to NPs) was used to determine statistical significance (*, $p < 0.05$; **, $p < 0.01$; ***, $p < 0.001$).

